References

[1] Connor, M. A., "Optimization of a Lateral Turn at Constant Height," *AIAA Journal*, Vol. 5, No. 7, Feb. 1967, pp. 335–338.

[2] Bryson, A. E. and Lele, M. L., "Minimum Fuel Lateral Turns at Constant Altitude," *AIAA Journal*, Vol. 7, No. 3, March 1969, pp. 559–560.

[3] Bryson, A. E. and Hedrick, J. K., "Minimum Time Turns for a Supersonic Aircraft at Constant Altitude," *Journal of Aircraft*, Vol. 8, No. 3, March 1971, pp. 182–187.

[4] Bryson, A. E. and Hedrick, J. K., "Three Dimensional, Minimum-Fuel Turns for a Supersonic Aircraft," AIAA Guidance, Control, and Flight Mechanics Conference, Hempstead, N.Y., Aug. 1971.

[5] Beebee, W., "Time Optimal Co-ordinated Turns Using Energy Methods," Measurement Systems Laboratory Rept, May 1970, MIT, Cambridge, Mass.

[6] Kelley, H. J. and Edelbaum, T. N., "Energy Climbs, Energy Turns, and Asymptotic Expansions," *Journal of Aircraft*, Vol. 7, No. 1, Jan.-Feb. 1970, pp. 93–95.

[7] Boyd, J. R. and Christie, T. P., "Energy Maneuverability Theory and Applications," Paper for 12th Annual Air Force Science and Engineering Symposium, Oct. 1965.

[8] Hedrick, J. K., *Optimal Three-Dimensional Turning Maneuvers for Supersonic Aircraft*, Ph.D. dissertation, 1971, Dept. of Aeronautics and Astronautics, Stanford Univ., Stanford, Calif.

[9] Bryson, A. E., Desai, M. N., and Hoffman, W. L., "The Energy State Approximation in Performance Optimization of Supersonic Aircraft," *Journal of Aircraft*, Vol. 6 Nov.-Dec. 1969, pp. 481–487.

FEBRUARY 1972 J. AIRCRAFT VOL. 9, NO. 2.

External Drag of Fuselage Side Intakes

M. D. DOBSON* AND E. L. GOLDSMITH†
Royal Aircraft Establishment, Bedford, England

Results of experiments designed to measure the external drag associated with varying internal flows of fuselage side intakes are presented. At subsonic speeds, cowl lip radius is found to affect drag at full internal flow but its influence decreases as flow is reduced. Conversely, cowl external profile is of significance in terms of spillage drag but does not influence the full flow drag. For a particular rectangular supersonic intake, the addition of swept endwalls is found to affect both full flow and spillage drags. At supersonic speeds, changes in full flow drag with variation of compression surface geometry are compared with those predicted from consideration of shock geometry changes. For supersonic intakes, spillage drag is found to vary in the manner predicted by calculation but for pitot intakes at $M_\infty = 2.0$, calculation over predicts spillage drag because, it is thought, of benefits which arise from the interaction of the intake shock with the fuselage boundary layer. Using a combination of measurement and calculation, pressure drags have been obtained for simple wedge boundary-layer diverters and for two intake configurations at full flow. These latter are compared with values calculated on the basis of isolated pitot intakes.

Nomenclature

A = area
C_D = drag coefficient
D = drag
h = height
M = Mach number
p = static pressure
q = dynamic pressure
r = radius
Re = Reynolds number
γ = ratio of specific heats
δ_2 = compression surface angle (see Fig. 2b)
θ = angle
Δ = increment

Subscripts

BAL = balance
BASE = model base
C = cowl
D = diverter
e = entry (defined in Fig. 2c)
E = external
f = skin-friction
$(F+C)$ = fuselage plus canopy
h = highlight (defined in Fig. 2c)
i = inlet (defined in Fig. 2b)
I = internal
l = lip (defined in Fig. 2c)
L = local flow conditions external to the fuselage boundary layer
P = pressure
PRE = pre-entry
PRE 0 = pre-entry at full internal flow
R = ramp (defined in Fig. 2b)
SPILL = spillage
W = wave
x = duct internal measuring station
∞ = freestream station

Received January 12, 1971; revision received September 14, 1971. Shortened version of paper ICAS 70–49 presented at the 7th Congress of the International Council of the Aeronautical Sciences, Rome, Italy, September 1970.

Index categories: Aircraft Powerplant Design and Installation; and Aircraft and Component Wind Tunnel Testing.

* Principal Scientific Officer, Aerodynamics Department.

† Senior Principal Scientific Officer, Aerodynamics Department.

Introduction

MULTIMISSION combat aircraft, as their name implies, have to perform efficiently over a wide range of flight speed, engine speed and aircraft attitude. They must be able to operate at sea level at high-subsonic or low supersonic speeds to evade detection, to climb to high altitude for inter-

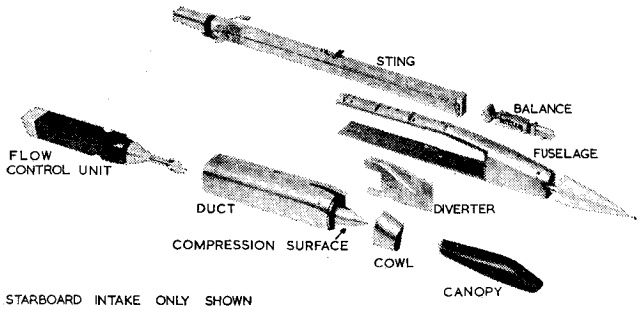

Fig. 1 Photograph of exploded model.

ception purposes at Mach numbers from 2.0 to 2.5 and to cruise at high altitude at $M_\infty = 0.6$ to 0.8 to achieve long range.

Most of these aircraft designs feature twin engines mounted in the fuselage and fed by air from intakes on the sides of the fuselage, exhausting via twin nozzles at, or upstream of the end of the fuselage. As is well known, the correct representation of intake flow and nozzle exhaust flow, and the simultaneous measurement of external forces poses one of the major problems in wind-tunnel testing. Often the only way to obtain accurate measurements (particularly of drag) is to study the effects of intake or exhaust flow representation on partial models that do not fully represent the complete aircraft. Results from these tests then have to be related to tests on complete aircraft models where probably the intake and exhaust flows have not been simulated correctly.

This paper presents results of wind-tunnel tests made with one particular partial model which measures drag at subsonic and supersonic speeds of twin intakes on the sides of a fuselage. The technique used is that of mounting the fuselage plus intakes on a balance, earthing the intake flow control valves and measuring balance, internal and base drags to obtain external drag.

Test Details

A photograph of the model in exploded form is shown in Fig. 1. All tests were made with the fuselage datum at zero incidence in the 3ft × 3ft wind tunnel at values of Reynolds number shown in Table 1.

Various rectangular and semicircular intake configurations have been tested and in the discussion which follows results are selected to illustrate particular drag components and do not necessarily form a set of data that is consistent in terms of intake configuration. Intake geometries are not defined in detail but the main features of each particular configuration used are included with the results.

Measurements

Preliminary experiments were made to survey the fuselage flow in the plane of the intake. Fuselage boundary-layer profiles were measured over the span of the intake at both subsonic and supersonic speeds and the mean local Mach numbers of the flow, external to the boundary layer, at supersonic speeds are given in Table 2.

Three components of drag are measured which combine to give the total external drag coefficient of the model as

$$C_{D_E} = D_E/q_\infty 2A_e = C_{D_{BAL}} - C_{D_{BASE}} - 2C_{D_I} \qquad (1)$$

Table 1 Test Reynolds number (based on h_e and r_e, Fig. 2)

M_∞	Subsonic	1.41	1.71	2.00
$Re \times 10^{-6}$	0.52–0.78	0.36–0.46	0.28–0.39	0.21–0.29

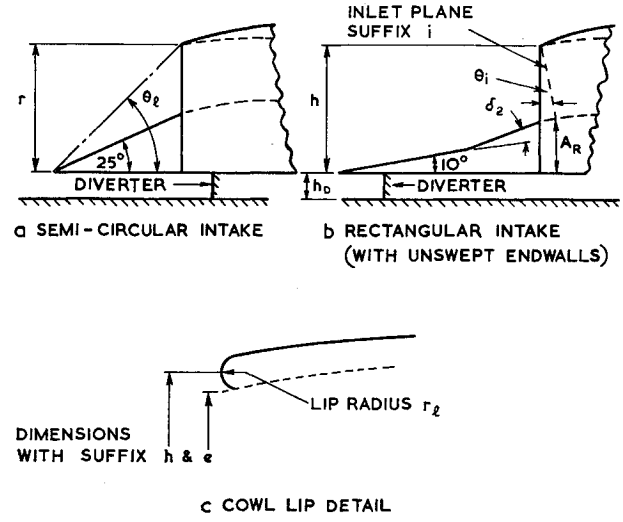

Fig. 2 Details of intakes.

where C_{D_E} is the total external drag coefficient, i.e., the sum of the drags of the unboattailed fuselage, the diverters and the two intake nacelles. $C_{D_{BAL}}$ is the drag coefficient measured by the strain gauge balance. $C_{D_{BASE}}$ is base pressure coefficient obtained from an area weighted integration of pressures measured by an array of forward facing tubes located close to the shrouded model base and supported from the sting. $2C_{D_I}$ is the sum of the measured internal drag coefficients of the two ducts.

The internal flow is controlled and measured by instrumentation which is earthed to the sting support and therefore the drag associated with it does not appear in the internal drag calculation. The equation used in the calculation of internal drag is

$$C_{D_I} = 2A_\infty/A_e - [(p_x - p_\infty) + \gamma p_x M_x^2]A_x/q_\infty A_e \qquad (2)$$

which gives the internal drag from a freestream station to the measuring station in the model duct. The internal instrumentation does not measure the skin-friction drag on the parallel duct wall between the measuring station and the exit. This quantity is calculated using flat plate skin-friction data.[1] To ensure sufficient accuracy in the measurement of internal mass flow, the model ducts and instrumentation have been calibrated[2] against a standard flow measuring device and for this the actual intakes were replaced by bell-mouths with 4:1 contraction ratio.

Discussion of Results at Subsonic Speeds

Maximum Intake Mass Flow

Experimental results are presented as curves showing the variation of total external drag with intake mass flow ratio. These curves are referred to as external drag curves. At subsonic speeds the maximum internal flow which can be achieved is limited by choking of the flow in the intake throat. The drag of the model at this condition is defined as the full flow drag and any change from this value, which results from a change of internal flow, is defined as spillage drag. It was not possible to pass sufficient flow in all of the intake configurations to achieve choking in the intake throat. For those

Table 2 Mean Mach numbers at intake plane

M_∞	1.41	1.71	2.00
M_L	1.46	1.75	2.01

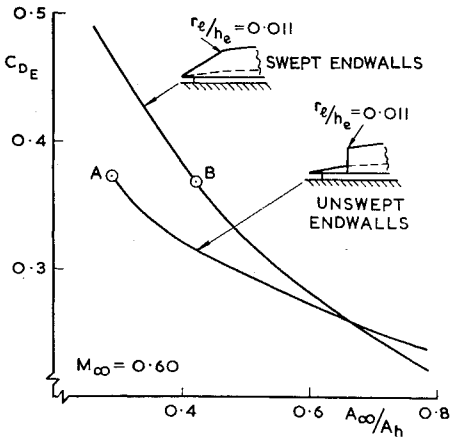

Fig. 3 Effect of swept endwalls on external drag of a rectangular intake.

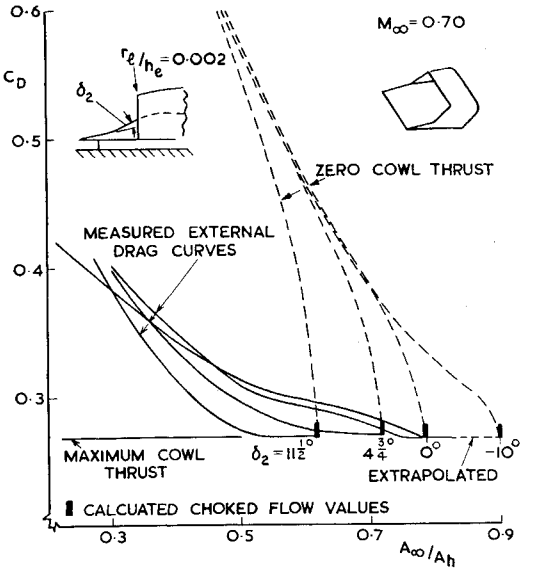

Fig. 4 Effect of change of compression surface geometry on external drag of a rectangular intake.

intakes in which it was possible, the measured values of flow agreed with calculation to within about 1%. In other cases, when the maximum internal flow which could be obtained was limited by duct exit size, measured external drag results are extrapolated to the conditions calculated for choked flow.

Effect of Swept Endwalls—Rectangular Intake

Figure 3 illustrates the effect on drag of changing from an unswept to a swept endwall shape. Swept endwalls give a lower value of drag at full flow but a considerably steeper rise in drag as flow is reduced. Swept endwalls have a larger wetted area and thus some (small) increase in skin-friction drag would be expected. However, in this particular design, they have the effect of fairing the steep external profile of the unswept endwall configuration and consequently of altering the local fineness ratio. It is not clear whether this or the fact that swept enwalls prevent lateral flow, is the reason for the lower measured drag at full flow. Under spilling conditions prevention of lateral flow by swept endwalls means that, to a large extent, the air that is spilled affects only the cowl. At points A and B on Fig. 3 the two configurations produce similar values of external drag for a difference in internal flow of about $\Delta A_\infty/A_h = 0.13$. Corresponding cowl surface flow patterns (not included here) indicate a similar extent of flow separation in the two cases and thus similar values of flowspilled over the cowl and cowl drag might be expected. If this is so, the difference noted in internal flow is achieved by sideways spillage over the unswept endwalls for no penalty in drag. This might be expected because firstly, the endwalls are operating at relatively low spillage and secondly, their external profile has a high slope.

Effect on Drag of Varying Compression Surface Geometry

External drag curves for rectangular and semicircular intakes with sharp lipped cowls are shown in Figs. 4 and 5, respectively. In each case results for various configurations of compression surface are included and these show that the external drag at full flow is virtually invariant with compression surface geometry. Thus, as has been observed previously[3] substantial flow spillage may be achieved with little drag penalty provided that the compression surface is adjusted to maintain a high Mach number at the intake throat.

Included on Fig. 4 is a curve (annotated as maximum cowl thrust) showing the variation of spillage drag with internal flow calculated on the assumption of complete cancellation of pre-entry drag by thrust forces developed on the cowl. This is simply a curve of constant drag drawn at the mean of the full flow drag levels of the measured results. Also included are curves (annotated as zero cowl thrust) which show the variation of spillage drag calculated on the assumption of no change in cowl thrust as internal flow is reduced. These curves show the total pre-entry drag, $C_{D_{PRE}}$, calculated by[4] analysis of the forces for a control volume bounded by the internal flow between a station at infinity upstream and the inlet station i (see Fig. 2) where

$$C_{D_{SPILL}} = C_{D_{PRE}} = (p_m - p_\infty)\, 1/q_\infty\, A_R/A_e + [q_i + \tfrac{1}{2}(p_i - p_\infty)]\, 2/q_\infty\, A_i/A_e \cos\theta_i - 2\, A_\infty/A_e \quad (3)$$

and it is assumed that $p_m = (p_i + p_\infty)/2$.

Effect of Cowl lip Radius and External Profile

This has been measured for both rectangular and semicircular intake configurations and external drag curves are shown in Fig. 6. In each case three cowls were tested, in which the different lip radii were followed by initial external profiles that were similar (i.e., parallel to each other) to a point about $0.7h_e$ downstream from the lip (Fig. 6). Aft of this point, differences were introduced to allow the cowls to blend into the same maximum section.

Results for the rectangular intake indicate that at high-internal flow, values of external drag for the sharp lipped cowl

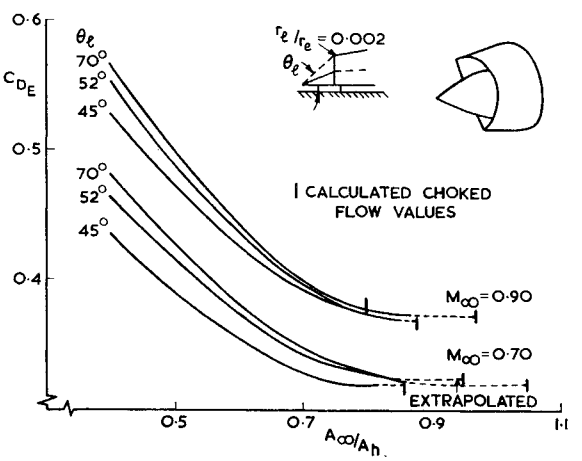

Fig. 5 Effect of change of position of compression surface on external drag of a semicircular intake.

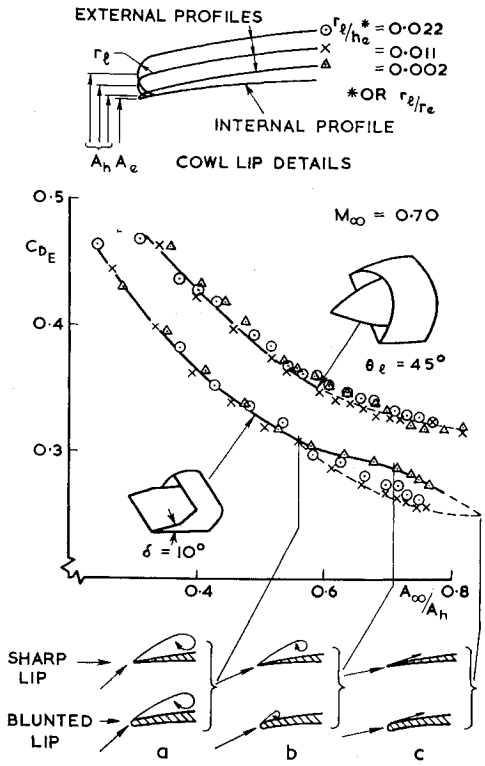

Fig. 6 Effect of cowl lip radius on external drag.

are higher than those for blunted lip cowls. As spillage is increased the difference becomes smaller and at spillages greater than $\Delta A_\infty/A_h = 0.15$ to 0.20 below full flow, drag is no loger sensitive to lip radius.

Evidence (not included here) of oil flow tests on the external cowl surface of a rectangular intake at $M_\infty = 0.7$, indicates that at low spillage the flow is characterised by a small bubble separation at the lip with attached streamwise flow over the remainder of the cowl. It is presumably the extent of this separation which determines the cowl drag, and thus the value of total external drag at full flow. The mass flow ratio at which flow separation at the cowl lip occurs will depend on both lip geometry and the incidence of the lip to the local flow direction which will, in turn, depend on the spill flow quantity and the compression surface geometry. Cowl flow conditions which could account for the measured changes in drag are sketched on Fig. 6. Condition (c), at which the flow may be attached for both cowls is not intended as a true extrapolation of the measured results but is drawn to illustrate that little difference in drag would be expected at this condition.

Results included in Fig. 6 for the semicircular intake configuration indicate that there is little effect of cowl lip radius on either the drag at full flow or the spill drag. On the basis of the preceding discussion this would indicate that at the full flow condition for this configuration, cowl flow separation is present for each lip, corresponding to condition (a) noted for the rectangular intake.

External drag curves for two rectangular cowls with rounded corners which have similar lip radii but different subsequent external profiles are shown in Fig. 7. These results illustrate that in this case the values of external drag at full flow are similar but the spill drag characteristics are different.

The evidence of the results illustrated previously therefore indicates that the cowl drag at full flow is largely dependent upon the radius at the cowl lip whereas the spillage drag characteristic is more dependent on the subsequent external profile of the cowl.

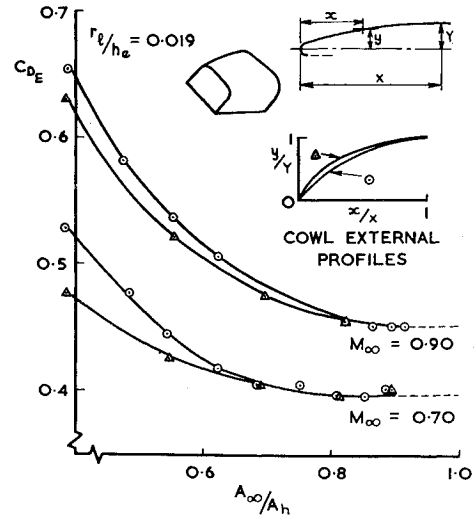

Fig. 7 Effect of cowl external profile on external drag.

Results at Supersonic Speeds

Changes in Drag at the Full Flow Condition

Differences in drag at full flow between the semicircular intake with and without the half-cone compression surface are plotted as a function of lip position angle θ_l in Fig. 8. The increase in drag as the cone shock moves forward of the cowl lip is in good agreement with the variation of pre-entry drag,[5] calculated by integration of the pressures acting on the boundary of the entering stream tube between the cone shock and the intake. However, there does appear to be a constant increment, particularly at $M_\infty = 2.00$, not allowed for in the calculation which could be due to the effect of the cone shock pressure rise on the wedge diverter. The measured increment for a sharp lipped configuration ($\Delta C_D = 0.02$–0.04) is about one-third of that which would be calculated on the simple basis of pressure rise times diverter projected frontal area.

As no rectangular pitot version of this intake was tested,

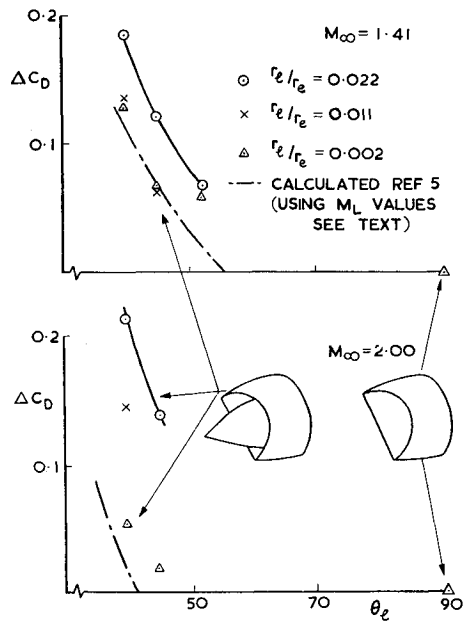

Fig. 8 Drag of semicircular intake at full flow—increments due to change in lip position angle.

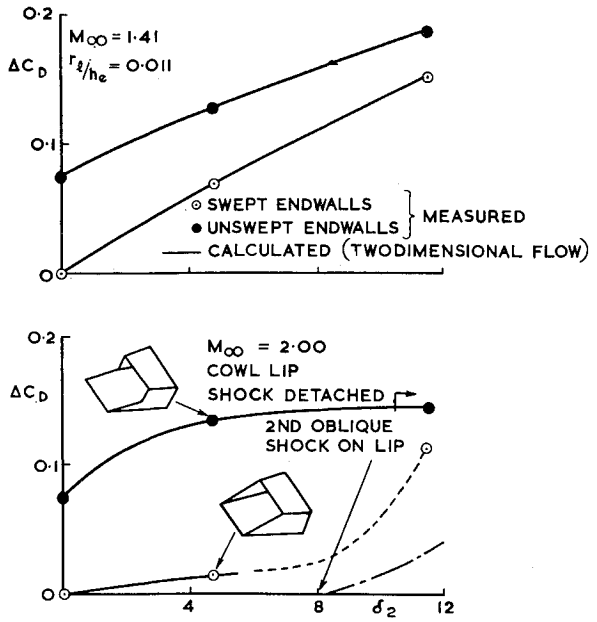

Fig. 9 Drag of rectangular intake at full flow—increments due to change in second wedge angle.

changes in drag shown in Fig. 9 are referred to the value for the configuration in which $\delta_2 = 0°$ (i.e., a single 10° wedge). For the configuration with swept endwalls at $M_\infty = 2.00$, drag increments measured for $\delta_2 = 4.75°$ and 11.5° are greater than the changes in pre-entry drag predicted by calculation. This discrepancy might be expected, since measured mass flows were lower than those predicted for these cases.

Changing endwalls from swept to unswept does not alter the total cowl projected area but, as mentioned earlier, does alter the endwall external profile considerably, for instance, in the region close to the fuselage the initial slope of the cowl changes from about 11°–30°. A rough calculation of the change in cowl wave drag[6] for this change of profile at $M_\infty = 2.00$ gives $\Delta C_D = 0.087$. This is reasonably close to the measured change $\Delta C_D = 0.075$. This measured increment will contain the drag associated with the additional spillage over the unswept endwalls. Assuming this is similar to that calculated for two dimensional forespillage[7] the drag, for say 5% spillage, would be about 0.012.

Spillage Drag

Drag coefficient is plotted as a function of intake mass flow for the semicircular Pitot intake in Fig. 10. Measured values of spillage drag (i.e., increments relative to the values of drag at full flow) are shown and may be compared with two curves obtained by calculation. The first shows the spillage drag calculated[8] simply by multiplying the spillage area ($A_h - A_\infty$) by the pressure rise across a normal shock, and the second shows the pre-entry drag obtained by calculation of the change of momentum in the internal flow between freestream and the inlet. Comparing slopes of the measured and calculated curves (i.e., the rate of drag rise with spillage) reasonable agreement is achieved at $M_\infty = 1.71$ (Fig. 10b) but not at the other Mach numbers. In general the method of calculating spillage drag[8] is known to give an overestimate at low-supersonic Mach numbers (e.g., $M_\infty = 1.41$) where it underestimates the favourable changes in cowl drag with spillage. A possible explanation of the lower measured slope at $M_\infty = 2.0$ may be the interaction between the intake shock and fuselage boundary layer which provides a branched shock configuration typically as sketched in Fig. 10c. A calculation may be made of the pre-entry drag associated with supersonic forespillage around a wedge[7] by assuming the separation resulting

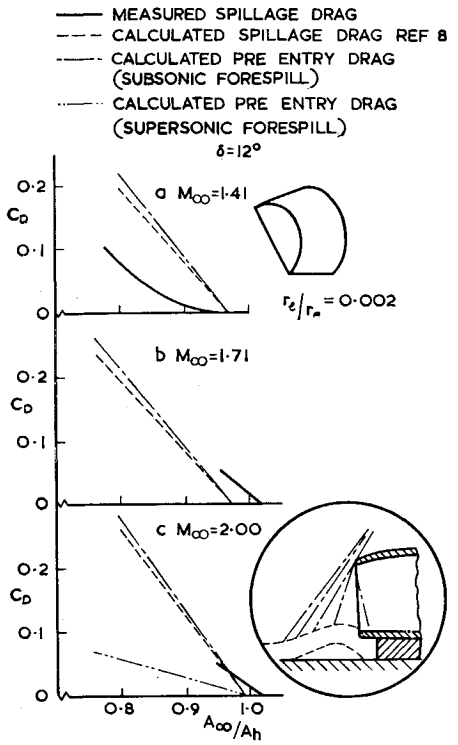

Fig. 10 Variation of spillage drag with mass flow ratio for a semicircular Pitot intake.

from the interaction as being equivalent to a 12° wedge (approximately the angle of the separated flow region). A curve of spillage drag calculated in this way is included on Fig. 10c and the slope of the measured curve compares more favourably with this than with that calculated assuming subsonic forespillage behind a normal shock. When a half-cone compression surface is introduced into the semicircular intake, spillage drag has been predicted by the methods of Ref. 9. In this reference drag is calculated from the external shock pattern which is itself obtained from consideration of the balance between internal and spilled flows. Results at $M_\infty = 2.0$ are shown in Fig. 11 and for a lip angle position of $\theta_l = 40°$, there is good agreement between measured and predicted slopes of the spillage drag curves. Good agreement is also obtained between the measured and predicted mass flow ratios at which buzz occurs according to the Ferri criterion,[10] i.e., when the vortex sheet from the intersection of the conical shock and the detached normal shock crosses the cowl lip. When θ_l is greater than the cone shock angle θ_w, the intersec-

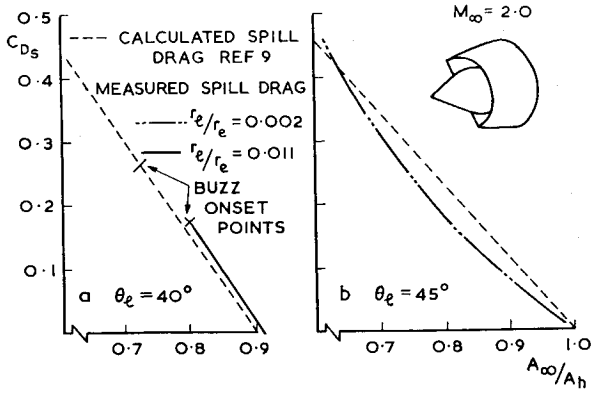

Fig. 11 Variation of spillage drag with mass flow ratio for a semicircular centre-body intake.

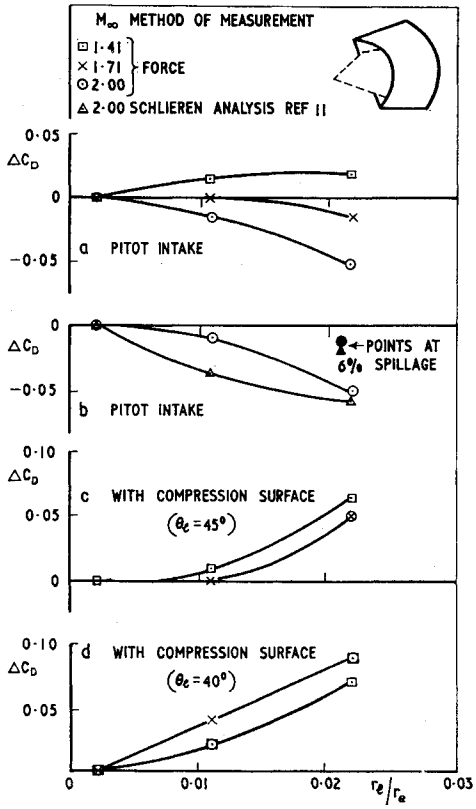

Fig. 12 Drag increment resulting from increase of cowl lip radius at supersonic speeds.

tion point between the cone shock and the detached shock in front of the cowl lip is always within the intake bounding streamline and in this case, spillage drag is predicted exactly as for the pitot intake. This condition exists at $M_\infty = 2.00$ when $\theta_l = 45°$ ($\theta_w = 42.5°$) and Fig. 11b shows good agreement between the slopes of measured and calculated spill drag curves. This is in contrast to results for the pitot intake, discussed previously and illustrated in Fig. 10c and it is evident that, in this case, the interaction of the intake terminal shock with the external boundary layer does not seriously modify the flow pattern. This is either because of the lower Mach number of the terminal shock or because the interaction is inhibited by the presence of a compression surface.

Changes of drag at full flow with increase in cowl lip radius for a semicircular Pitot intake are shown in Fig. 12a. At $M_\infty = 1.41$ drag increases with increasing bluntness of the lip, at $M_\infty = 2.00$ it decreases. In addition to force measurements, at $M_\infty = 2.00$ increments in drag due to lip bluntness have been calculated from analysis of the bow shock shape[11] measured from schlieren photographs. These drag increments are shown in Fig. 12b and are seen to compare well with force measurements. A comparison has also been made when the intake (with $r_l/r_e = 0.022$) is spilling 6% of the internal flow and again agreement between the two methods of measurement is very good.

When a compression surface is added to this intake the increment in drag (force measurements only) increases with increasing cowl lip radius at all Mach numbers, Fig. 12c and 12d. This trend has also been recorded for isolated axisymmetric intakes with[12] and without[13] a conical compression surface. It is difficult from this evidence to decide whether the difference in behaviour between the present intake with and without a compression surface is intrinsic or whether it is due to changes in interference effects associated with the proximity of the intake to the fuselage boundary layer and to the wedge diverter.

Diverter Drag

To evaluate the drag associated with a wedge shaped diverter for the fuselage boundary layer, tests were made using rectangular intakes with three values of diverter depth, h_D (see Fig. 2a and 2b), giving values of $h_D/h_e = 0$, 0.111 and 0.190.

When $h_D/h_e = 0$ the compression surface leading edge is in contact with the flat fuselage side and the drag associated with the area upstream of this, which is wetted by the internal flow, is measured as part of the internal drag. The skin-friction drag associated with this area may be calculated[1] and the drag values measured at $h_D/h_e = 0$ corrected accordingly. Table 3

Table 3 Diverter drag coefficients

		M_∞				
	h_D/h_e	0.60	0.85	1.41	1.71	2.00
Datum drag	0	0	0	0	0	0
Skin-friction drag[a] ($h_D/h_e = 0$ correction)	...	0.023	0.022	0.022	0.022	0.021
Skin-friction drag increment	0–0.111	0.033	0.032	0.032	0.031	0.031
Skin-friction drag total increment	0–0.111	0.056	0.054	0.054	0.053	0.052
Measured drag increment	0–0.111	0.047	0.046	0.072[b]	0.069[b]	...
Skin-friction drag increment	0.111–0.190	0.009	0.009	0.009	0.009	0.009
Skin-friction drag total increment	0–0.190	0.065	0.063	0.063	0.062	0.061
Measured drag increment	0–0.190	0.059	0.056	0.113	0.116	0.097
Pressure drag of diverter	0.190	$\simeq 0$	$\simeq 0$	0.050	0.054	0.036
Diverter pressure drag coefficient based on diverter frontal area (C_{DD})		$\simeq 0$	$\simeq 0$	0.084	0.090	0.060

[a] All skin-friction drag increments have been calculated using flat plate data.[1] Some reservation must therefore be placed on the accuracy of increments calculated because of some three dimensional surfaces which are involved.

[b] In these cases some of the external boundary layer is ingested by the intake but no correction has been made for the consequent small part of external drag which has been included in the internal drag measurements.

Table 4 Drag analysis—model with rectangular intakes

M_∞	0.60	0.70	0.80	0.90	1.41	1.71	2.00
					Drag coefficients		
Fuselage plus canopy drag ($C_{D_{(F+C)}}$)	0.151	0.151	0.160	0.191	0.442	0.416	0.454
Installation skin-friction drag (C_{D_f}(INST))	0.093	0.092	0.088	0.085	0.074	0.073	0.072
Diverter wave drag (C_{D_W}(DIV))					0.057	0.062	0.042
Pre-entry drag ($C_{D_{PRE\ 0}}$)					0.109	0.059	0.035
Total	0.244	0.243	0.248	0.276	0.682	0.610	0.603
Measured drag (C_{D_E})	0.239	0.250	0.251	0.286	0.785	0.820	0.830
Installed cowl pressure drag (C_{D_C}(INST))	$\simeq 0$	$\simeq 0$	$\simeq 0$	0.010	0.103	0.210	0.227
Estimated cowl wave drag					0.211	0.171	0.151

Table 5 Drag analysis—model with semicircular Pitot intake

M_∞	0.60	0.70	0.80	0.90	1.41	1.71	2.00
					Drag coefficients		
Fuselage plus canopy drag	0.148	0.149	0.158	0.188	0.434	0.409	0.447
Installation skin-friction drag	0.103	0.102	0.098	0.096	0.084	0.084	0.082
Diverter wave drag					0.056	0.061	0.041
Pre-entry drag					0	0	0
Total	0.251	0.251	0.256	0.284	0.574	0.554	0.570
Measured drag	0.295	0.299	0.300	0.329	0.720	0.770	0.795
Installed cowl pressure drag	0.044	0.048	0.044	0.045	0.146	0.216	0.225
Estimated cowl wave drag					0.207	0.167	0.148

shows increments in drag, measured from a datum level at $h_D/h_e = 0$, due to changes in h_D and also the associated changes in skin-friction drag. The difference between the two gives an indication of the diverter pressure drag.

Installed Intake Pressure Drag

Methods are available by which the wave drag of ducted bodies in supersonic flow may be predicted. These methods usually apply to idealised configurations and it is of interest to know whether predictions using these data for practical fuselage shapes and installed intake configurations will be of sufficient accuracy to be of use in design. An attempt has been made to study this by using a combination of measured drag and estimated skin-friction drag (calculated using flat plate skin-friction data[1]) to arrive at a value of pressure drag which may then be compared with predicted value. This analysis has been done over the freestream Mach number range 0.60–2.00 and results are presented in Tables 4 and 5.

In Table 4 the drag analysis is given for the model with rectangular intakes with unswept endwalls, $r_1/h_e = 0.022$ and $\delta_2 = 0°$. Using the notation indicated in this table the installed cowl pressure drag C_{D_C}(INST) is given by

$$C_{D_C}(\text{INST}) = C_{D_E} - \{C_{D_{(F+C)}} + C_{D_f}(\text{INST}) + C_{D_W}(\text{DIV}) + C_{D_{PRE\ 0}}\} \quad (4)$$

where C_{D_f}(INST) is the nacelle installation skin-friction drag coefficient, C_{D_W}(DIV) is the diverter pressure drag coefficient related to this installation using the values of C_{D_D} given in Table 3, and $C_{D_{PRE\ 0}}$ is the calculated pre-entry drag at the condition of maximum measured mass flow, assuming that the intake terminal shock is attached to the lip and thus all flow is spilled supersonically. A similar drag analysis is given in Table 5 for the model with semicircular sharp lipped pitot intakes. For both of the aforementioned configurations cowl wave drag has been estimated from Ref. 6, which uses a combination of slender body and quasi-cylinder theories and assumes the internal flow to have no influence on wave drag. For both of these configurations the experimentally derived pressure drag coefficients are similar and increase with increasing supersonic freestream Mach number, whereas the estimated wave drag coefficients do not. In the worst case, at $M_\infty = 1.41$ for the rectangular intake, the difference between the two values is just less than 14% of the measured total external drag.

At subsonic speeds this analysis gives a cowl pressure drag coefficient of approximately zero for the rectangular intake configuration but about 0.045 for the semicircular configuration. The installation skin-friction drag is similar in the two cases but the measured drag is higher for the semicircular intake configuration. Both intake designs have approximately the same capture area and both blend into similar maximum sections at approximately the same distance downstream from the lip. However local cowl external profiles are different, particularly in the regions close to the fuselage and it could be that the presence of the intakes affects the pressure distribution on the fuselage and thus its drag, differently in the two cases. With this method of analysis any interference effects are not isolated but are charged to the cowl which could account for the differences noted in the pressure drags. The same applies to the supersonic results as again any interference effects are charged to the cowl and this may account for the conflicting trends of wave drag with Mach number when compared with estimates which are based on the case of an isolated intake. The difficulties in computing transonic pressure distributions are well known but work is currently being done on the present model configurations to compute pressure distributions in supersonic flow and from this, some idea may be gained of the magnitude of any interference drag.

Conclusions

Some results are presented of an experiment designed to measure the drag associated with fuselage side intakes at subsonic and supersonic speeds. The model enables a range of intake configurations to be tested and the accuracy of measure-

ment is found to be adequate for the determination of components of external drag resulting from relatively small variations in intake and installation geometry. Drag at full flow as well as drag due to spillage has been measured. The effect of changing endwall geometry of a rectangular intake has been examined and the effects of cowl lip radius, cowl external profile and compression surface geometry have been investigated for both rectangular and semicircular types of intake.

Using the experimental data and skin-friction drag estimates, the wave drag of a wedge shaped diverter for the fuselage boundary layer has been derived and the wave drag of installed intakes has been derived in a similar way. Results for the latter are found to show some differences from estimates which are based on the case of isolated intakes and it is thought that this could result from installation interference effects which are not currently accountable.

References

[1] Smith, K. G., "Methods and Charts for Estimating Skin-Friction Drag in Wind Tunnel Tests with Zero Heat Transfer," CP 824, 1964, British Aeronautical Research Council, National Physical Laboratory, Teddington, Middlesex, England.

[2] McGregor, I., "The Characteristics and Calibration of Two Types of Airflow Metering Device for Investigating the Performance of Model Air Intakes," Royal Aircraft Establishment, Bedford, England, to be published.

[3] Mount, J. S., "Additive Drag on Inlet Cowls and Its Effect on Aircraft Performance," AGARDograph 103, 1965, North American Aviation, Los Angeles, Calif.

[4] Neale, M. C., "The Drag of Variable Ramp Intakes at High Subsonic Mach Number," Note 653, 1967, National Gas Turbine Establishment, Pystock, Hants, England.

[5] Fraenkel, L. E., "Some Curves for Use in the Calculations of the Performance of Conical Centre-Body Intakes at Supersonic Speeds at Full Mass Flow," CP 108, 1951, British Aeronautical Research Council, National Physical Laboratory, Teddington, Middlesex, England.

[6] Fraenkel, L. E., "Curves for Estimating the Wave Drag of Some Bodies of Revolution Based on Exact and Approximate Theories," CP 136, 1952, British Aeronautical Research Council, National Physical Laboratory, Teddington, Middlesex, England.

[7] Dutton, R. A. and Goldsmith, E. L., "The Drag of Some Wedge Centre-Body Intakes at Mach Numbers of 1.56, 1.86 and 2.14," CP 968, 1966, British Aeronautical Research Council, National Physical Laboratory, Teddington, Middlesex, England.

[8] Seddon, J., "Note on the Spillage Drag of Pitot-Type Air Intakes at Transonic Speeds," TN 2315, 1954, Royal Aircraft Establishment, Farnborough, Hants, England.

[9] Goldsmith, E. L. and Griggs, C. F., "The Estimation of Shock Pressure Recovery and External Drag of Conical Centre-Body Intakes at Supersonic Speeds," R and M 3035, 1959, British Aeronautical Research Council, National Physical Laboratory, Teddington, Middlesex, England.

[10] Ferri, A. and Nucci, L., "The Origin of Aerodynamic Instability of Supersonic Inlets at Sub-Critical Conditions," RM L50 K36, 1957, NACA.

[11] Pugh, P. G. and Ward, L. C., "The Estimation of Zero Incidence Forebody Pressure Drag Coefficients of Axi-Symmetric Bodies from Measured Bow Shock Shapes," Rept. Aero 1245, 1967, National Physical Lab., Teddington, Middlesex, England.

[12] Goldsmith, E. L. and Griggs, C. F., "A Comparison of the Estimated and Measured Performance of Conical Centre-Body Intakes at Mach Numbers from 2.14 to 3.27," R and M 3035, 1953, British Aeronautical Research Council, National Physical Laboratory, Teddington, Middlesex, England.

[13] Fraenkel, L. E., "The External Drag of Some Pitot Type Intakes at Supersonic Speeds, Part II," Rept. Aero 2422, 1951, Royal Aircraft Establishment, Farnborough, Hants, England.